DOAS tomography for the retrieval of trace gas profiles from satellite-based UV-Vis limb spectra

Zijun Wang (汪自军), Shengbo Chen (陈圣波)*, Chunyan Yang (杨春燕), and Mingchang Wang (王明常)

College of Geo-Exploration Science and Technology, Jilin University, Changchun 130026, China

**Corresponding author: chensb@jlu.edu.cn*

Received August 5, 2010; accepted October 14, 2010; posted online January 28, 2011

A new method is employed for retrieving the profiles of trace gas number densities from satellite-based ultraviolet-visible (UV-Vis) spectra of scattered sunlight, which are recorded from the limb atmosphere over a range of tangent heights. The slant column abundances of trace gas along the lines of sight (LOSs) are obtained by differential optical absorption spectroscopy (DOAS), and the tomographic technique is applied to such column abundances to retrieve two-dimensional (2D) concentration profiles. For validation of the tomographic technique, the slant column abundances are simulated by a tested 2D NO_2 profile set with latitudes from 90°S to 90°N between altitudes of 0 and 100 km, and the retrieval of number density profiles on 1-km grids is performed. The results suggest that between ±80°, the retrieved structure is almost the same as the test data. According to the comparison of the selected cross sections of the vertical profiles between retrieved and true concentrations, the NO_2 number densities have been retrieved with an accuracy of 15% or better and 5% for altitudes between 25 and 40 km. The validation of the retrieved data shows good agreement between the retrieved and true profiles.

OCIS codes: 010.1280, 010.1310, 010.5620, 280.1310.

doi: 10.3788/COL201109.020101.

Multiple satellite instruments have been developed to date to measure the limb scattered spectra at ultraviolet-visible (UV-Vis) wavelengths. The limb remote sensing technique allows for the retrieval of trace gas profiles at a vertical resolution comparable to that of occultation measurements, but with significantly better global coverage[1]. A number of satellite instruments that measure limb radiances with the goal of deriving the vertical profiles of trace gases have recently been launched. These instruments include OSIRIS on the Odin satellite[2] and SCIAMACHY on Envisat[3]. In China, a prototype of grating dispersion type UV-Vis limb imaging spectrometer has been designed by Xue *et al.*[4]

A number of methods for retrieving trace gas profiles from limb spectra have been proposed, including methods that retrieve information directly from the limb measurements and those that apply a spectral analysis technique to simplify the problem[5]. There are some spectral analysis techniques, e.g., methods applying iterative least-squares technique to column densities retrieved by differential optical absorption spectroscopy (DOAS)[6], and methods that combine DOAS and optimal estimation from limb scattered sunlight[7]. However, these methods can usually only retrieve one-dimensional (1D) profiles[8]. In order to get two-dimensional (2D) structures simultaneously from limb UV-Vis scattered spectra, a new method combining DOAS and tomography is employed.

Tomography is a technique that can recover the function distribution from integration along a series of lines or reconstruct the cross-section image of an object from observations along different directions[9,10]. In recent decades, it has been used to recover atmospheric structures from rocket tomographic measurement of satellite limb remotely sensed airglow or infrared emission spectra. Tomographic nadir satellite remote sensing was promoted by Fleming[11], and a rocket measurement of N_2^+ 391.4-nm emission in an auroral arc was retrieved by tomography[12]. More recently, mesospheric ozone profiles have been successfully retrieved by tomography and ozone optical chemistry model from the oxygen atmospheric infrared band emission[13,14].

In this letter, the tomographic technique for retrieving 2D profiles of trace gas is described, followed by a brief overview of column abundance obtained by DOAS from limb UV-Vis sunlight spectra. A test retrieval application with some comparisons between retrieved and true profiles illustrates that the tomographic technique is appropriate for investigating atmospheric species profiles.

The slant column abundance along each line of sight (LOS) is derived using the DOAS, which can remove spectral features that are smoothly varying components of wavelength[7]. For a single species in an inhomogeneous medium, the optical depth along the LOS through tangent height h_t is expressed as

$$\tau(\lambda, h_t) = \int \sigma(\lambda) n(h) \mathrm{d}s = \sigma(\lambda) \int n(h) \mathrm{d}s, \quad (1)$$

where $\sigma(\lambda)$ is the wavelength-dependent absorption cross section and $n(h)$ is the number density of the species at altitude h. Instead of the number density and path length, the slant column abundance along the LOS, which is denoted as C, is used:

$$C(h_t) = \int n(h) \mathrm{d}s. \quad (2)$$

For atmospheric limb conditions, Rayleigh and Mie scattering also contribute to the radiation extinction[5]. In addition, multiple-interest absorbing species, denoted as index i, must usually be included. With some rearrangement, the optical depth can be expressed as

$$\tau(\lambda, h_t) = -\ln\left[\frac{I(\lambda, h_t)}{I_0(\lambda)}\right]$$

$$= \sum_i \sigma_i(\lambda) C_i(h_t) + \tau_R(\lambda, h_t) + \tau_M(\lambda, h_t), \quad (3)$$

where $I(\lambda, h_t)$ is the measured intensity, $I_0(\lambda)$ is the unattenuated reference intensity of solar radiation, and subscripts "R" and "M" represent Rayleigh and Mie scattering, respectively. The key principle of the DOAS approach assumes that each of the absorption cross section can be separated into two components: one is slowly varying with wavelength, $\sigma_i^S(\lambda)$, and another is rapidly varying, $\sigma_i^D(\lambda)$, or the differential component. The total optical depth can then be represented as a sum of its own two components[6]—slowly varying optical depth and differential optical depth—in the following equation:

$$\tau(\lambda, h_t) = \sum_i \sigma_i^D(\lambda) C(h_t) + \sum_i \sigma_i^S(\lambda) C(h_t) + \tau_R(\lambda, h_t) + \tau_M(\lambda, h_t). \quad (4)$$

Both Rayleigh and Mie scattering are slowly varying with wavelength and are assigned to the slowly varying components of the optical depth.

The slowly varying component, which describes the general slope, corresponds to a smoothing of the total cross section and can be calculated with a polynomial piecewise fitting[5,7]. The differential cross section corresponds to the difference between the total and the smoothed cross sections. The same procedure is used to generate the differential optical depth.

The measured differential optical depth due to the differential cross sections is given as

$$\tau^D(\lambda) = \sum_i \sigma_i^D(\lambda) C(h_t) + E_D(\lambda, h_t), \quad (5)$$

where $E_D(\lambda, h_t)$ is the error in the differential optical depth caused by the measurement error of the instrument. The error has a mean of zero. If the count of the selected wavelength is more than that of the species, then slant column abundances can be calculated simultaneously through a least-squares fit of Eq. (5) with respect to C[5,7].

The application of tomographic retrieval techniques relies on the fact that all of the line integrals are available at over 180°[14], which is not available in limb remote sensing due to the solid nature of the Earth. Hence, a distinctive technique is required to recover 2D atmospheric constituent profiles.

Figure 1 is a typical limb geometry in the ascending (asc) node coordinate system, wherein the atmosphere is divided by shell layer and angular division represented by the atmospheric grid. For a single LOS, the slant column abundance can be expressed as a discrete form:

$$C_i = \sum_j n_j L_{i,j}, \quad (6)$$

where C_i is the column abundance along LOS i; n_j is the number density of cell j in atmospheric grid; and $L_{i,j}$ is the path length of LOS i through cell j.

Degenstein developed the following simple iterative equation[14]:

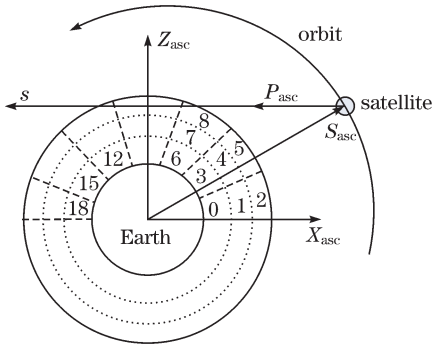

Fig. 1. Typical limb geometry.

$$n_j^{(k)} = n_j^{(k-1)} \sum_i \left(\frac{C_i}{C_{i,\mathrm{est}}^{(k-1)}} \beta_{i,j} \right), \quad (7)$$

where $n_j^{(k)}$ is the number density of cell j after the kth iteration, $\beta_{i,j}$ is the weighting factor defined as

$$\beta_{i,j} = \frac{L_{i,j}}{\sum_i L_{i,j}}, \quad (8)$$

C_i is the column abundance along LOS i from the observed spectra by the DOAS analysis. The estimated column abundance $C_{i,\mathrm{est}}$ is calculated by Eq. (6).

If $k = 1$, Eq. (6) can be substituted into Eq. (7) to derive the initial number density as follows:

$$n_j^{(1)} = \sum_i \left(\frac{C_i}{\sum_j L_{i,j}} \beta_{i,j} \right). \quad (9)$$

Thus, under the assumption that the profile is uniform only along each LOS, the actual initial estimates for this algorithm are the weighted averages over all the column densities.

For testing the tomographic technique, a number density profile of NO_2 of latitudes from 90°S to 90°N with altitudes between 0 and 100 km was selected as the true atmospheric structure. Based on this profile, column abundances of NO_2 of different images and different tangent heights were simulated. The number density in each atmospheric grid was then retrieved by tomography from the modeled column abundances.

The column abundance along the LOS can be calculated using Eq. (2); as shown in Fig. 1 in the atmospheric grid, the slant column abundance will be expressed as a discrete form, as shown in Eq. (6). In that equation, n_j corresponding to the number density of cell j is given by the test NO_2 profile. Another parameter $L_{i,j}$, which is the path length of LOS i through cell j, can be calculated according to the observed geometry shown in Fig. 1 if the satellite motion parameters and orientation parameters are known. The atmospheric NO_2 profiles bounded by angles 90° and −90° along the orbit track limit the angle range that the satellite scans the atmosphere. According to the geometry in Fig. 1, the upper and lower angles $\alpha_{\max}$ and $\alpha_{\min}$ that the satellite scans the atmo-

sphere are given by

$$\alpha_{\max} = 90^\circ - \arccos(R_{\min}/R_{\max}) - \arccos(R_{\min}/R_{\text{sat}}), \quad (10)$$

$$\alpha_{\min} = -90^\circ - [\arccos(R_{\min}/R_{\text{sat}}) - \arccos(R_{\min}/R_{\max})], \quad (11)$$

where the altitude of the bottom and top layers, $R_{\min}$ and $R_{\max}$, of the atmospheric grid are 6382 and 6482 km, respectively, and R_{sat} is the radius of the satellite chosen as 6978 km. Sequentially, we conclude that the satellite must make measurement from -103.775° to 56.070°.

The column abundances of NO_2 along 100 LOSs at 1279 measurements along the orbit track of the satellite were modeled from the test NO_2 profile set by Eq. (6) (see Fig. 2). The NO_2 number densities in Fig. 2(a) are almost zero at above 60 km and achieve the peak at about 35 km. The peak column abundances in Fig. 2(b) are along the lowest LOS and are zero at above 45 km.

Figure 3 shows the retrieved NO_2 profile by tomographic technique. It is apparent that even the initial estimate, which is based on Eq. (9), displays some of the structures shown in the input NO_2 profile. The final retrieved solution after 40 iterations of Eq. (7) is given in Fig. 3(b). The big error in both edges of the retrieved profile exists due to an insufficient limb scanning in these areas. The legend would be shown with the same scale if such errors are removed.

The accuracy of retrieval was evaluated by comparing the retrieved and true data sets. A distribution of difference between the retrieved and tested profiles was obtained from this comparison and fitted with a quadratic function (see Fig. 4). The bin of error distribution histogram was 0.1%. To remove the effect of edges,

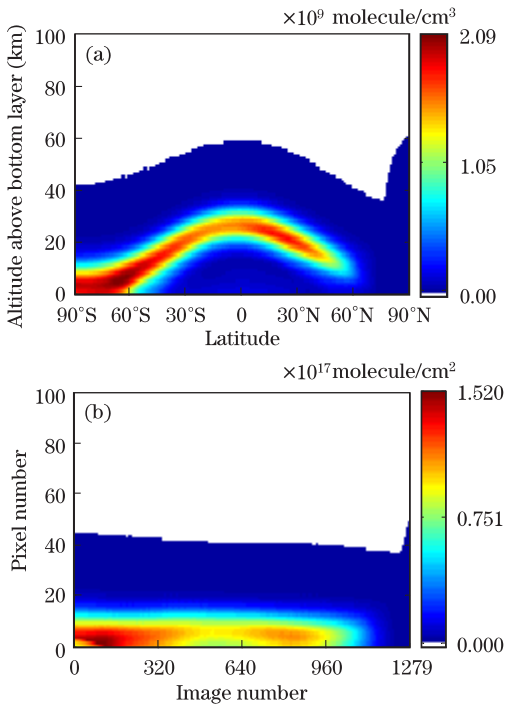

Fig. 2. (a) Test latitude-altitude NO_2 2D profile and (b) corresponding modeled NO_2 column abundance.

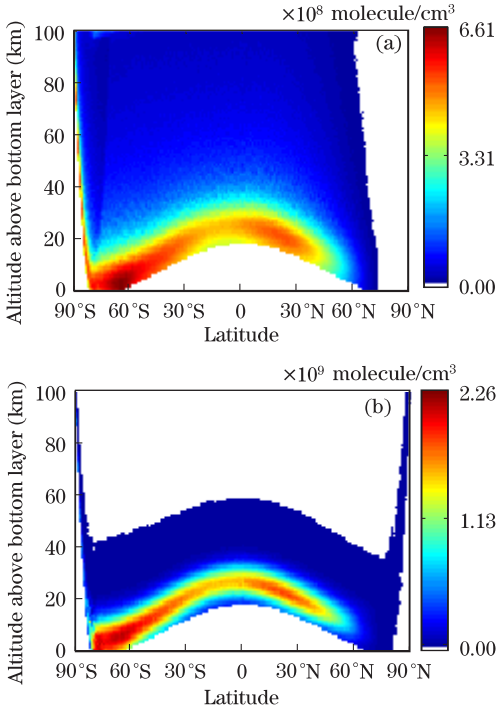

Fig. 3. (a) Initial estimate of the number density profile and (b) final estimate of the number density profile after 40 iterations.

the distribution was limited to ±20%. In Fig. 4, the full-width at half-maximum (FWHM) of the error distribution is 4.94%, and the offset of the peak percentage of quadratic fit from 0% is −0.39%. There is no significant improvement after about 40 iterations, thus the termination condition of inversion in this study is 40 iterations.

Figure 5 illustrates the difference between the retrieved and true profiles at three selected latitudes. The differences almost exist within ±15% and even less within ±5% at below 40 km.

In conclusion, a method for retrieving 2D trace gas profiles from satellite-based UV-Vis limb spectra has been presented. This method combines DOAS and the tomographic technique. It includes two steps: firstly, the slant column abundances along the LOS of different tangent heights are obtained by the DOAS approach, and secondly, the number densities are recovered from column abundances using the tomographic technique.

To validate this technique, a test application has been

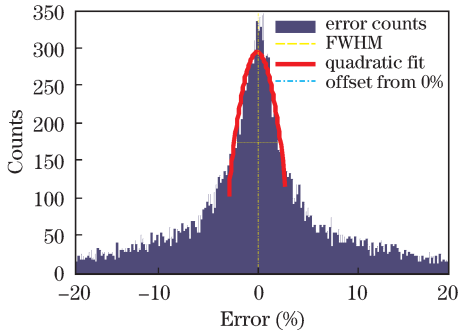

Fig. 4. Percentage error distribution between retrieved and tested profiles.

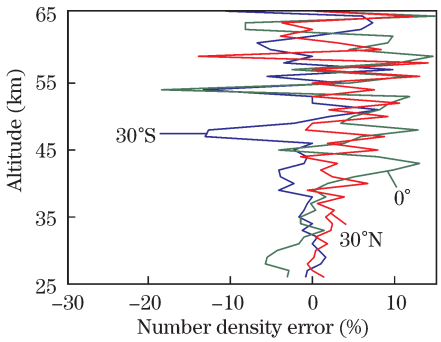

Fig. 5. Difference percentages between input and retrieved vertical profiles at three selected latitudes.

applied to 2D number density profile retrieval of NO_2. The column abundances are simulated from the input test number density profiles. The number densities with vertical resolution of 1 km are then derived by the DOAS tomography. The initial estimate of the profiles shows the structure of the true profiles, and the recovered profiles after 40 iterations illustrate good agreement with the input true profiles. Finally, the accuracy and comparison of retrieval are analyzed. The width of error distribution is 4.94%, and the offset of the peak from 0% is −0.39%. The differences are within ±15% between 25 and 65 km, and even less within ±5% at below 40 km.

The DOAS tomography and the application indicate that the retrieval is appropriate and highly accurate. This technique may be applied to satellite UV-Vis limb measurement, as observed by recent instruments such as OSIRIS and SCIAMACHY. Future applications of DOAS tomography to the UV-Vis region may provide atmospheric O_3, BrO, and OClO number density profiles as long as the appropriate spectral windows are selected.

This work was supported by the National "863" Program of China (No. 2006AA12Z102) and the Graduate Innovation Fund of Jilin University (No. 20091023).

References

1. D. A. Degenstein, A. E. Bourassa, C. Z. Roth, and E. J. Llewellyn, Atmos. Chem. Phys. **9,** 6521 (2009).
2. D. Murtagh, U. Frisk, F. Merino, M. Ridal, A. Jonsson, J. Stegman, G. Witt, P. Eriksson, C. Jiménez, G. Megie, and J. D. L. Noe, Can. J. Phys. **80,** 309 (2002).
3. A. J. M. Piters, K. Bramstedt, J.-C. Lambert, and B. Kirchhoff, Atmos. Chem. Phys. **6,** 127 (2006).
4. Q. Xue, S. Wang, and F. Li, Acta Opt. Sin. (in Chinese) **30,** 1516 (2010).
5. C. S. Haley, S. M. Brohede, C. E. Sioris, E. Griffioen, D. P. Murtagh, I. C. McDade, P. Eriksson, E. J. Llewellyn, A. Bazureau, and F. Goutail, J. Geophys. Res. **109,** 1 (2004).
6. I. C. McDade, K. Strong, C. S. Haley, J. Stegman, D. P. Murtagh, and E. J. Llewellyn, Can. J. Phys. **80,** 395 (2002).
7. K. Strong, B. M. Joseph, R. Dosanjh, I. C. McDade, C. A. McLinden, J. C. McConell, J. Stegman, D. P. Murtagh, and E. J. Llewellyn, Can. J. Phys. **80,** 409 (2002).
8. C. D. Rodegers, Rev. Geophys. Space Phys. **14,** 609 (1976).
9. C. Zhang and Y. Wang, Acta Opt. Sin. (in Chinese) **28,** 2296 (2008).
10. Y. Wang, X. Chen, H. Li, Q. Li, and D. Yu, Chinese J. Lasers (in Chinese) **36,** 2534 (2009).
11. H. E. Fleming, J. Appl. Meteoralogy **21,** 1538 (1982).
12. I. C. McDade, N. D. Lloyd, and E. J. Llewellyn, Planet Space Sci. **39,** 895 (1991).
13. J. T. Wiensz, "Ozone retrievals from the oxygen infrared channels of the OSIRIS infrared imager" M.S. Thesis (University of Saskatchewan, Saskatchewan, 2005).
14. D. A. Degenstein, "Atmospheric volume emission tomography from a satellite platform" PhD. Thesis (University of Saskatchewan, Saskatchewan, 1999).